Blue and red photoluminescence from $Al_2O_3:Ce^{3+}:Mn^{2+}$ films deposited by spray pyrolysis

2005 J. Phys.: Condens. Matter 17 3647

(http://iopscience.iop.org/0953-8984/17/23/016)

INSTITUTE OF PHYSICS PUBLISHING JOURNAL OF PHYSICS: CONDENSED MATTER

J. Phys.: Condens. Matter **17** (2005) 3647–3656 doi:10.1088/0953-8984/17/23/016

Blue and red photoluminescence from $Al_2O_3:Ce^{3+}:Mn^{2+}$ films deposited by spray pyrolysis

R Martínez-Martínez[1], M García-Hipólito[1], F Ramos-Brito[2], J L Hernández-Pozos[3], U Caldiño[3] and C Falcony[4]

[1] Instituto de Investigación en Materiales, Universidad Nacional Autónoma de México, PO Box 20-364, 01000 México, DF, Mexico
[2] Facultad de Ciencias Físico Matemáticas, UA de C, PO Box 60-C, Campo Redondo, 25280 Saltillo, Coahuila, Mexico
[3] Departamento de Física, Universidad Autónoma Metropolitana-Iztapalapa, PO Box 55-534, 09340 México, DF, Mexico
[4] Centro de Investigaciones y Estudios Avanzados del IPN, Departamento de Física, PO Box 14-7400, 7000 México, DF, Mexico

Received 14 October 2004, in final form 8 March 2005
Published 27 May 2005
Online at stacks.iop.org/JPhysCM/17/3647

Abstract

$Al_2O_3:Ce^{3+}:Mn^{2+}$ films deposited by the spray pyrolysis technique show blue and red emissions under ultraviolet light excitation. The blue emission is due to the de-excitation of Ce^{3+} ions from their excited state 5d to the split ground state ^2F. The usually weak red emission attributed to 3d → 3d de-excitation of Mn^{2+} is enhanced through an efficient energy transfer from Ce^{3+} to Mn^{2+} ions. The most probable mechanism of $Ce^{3+} \rightarrow Mn^{2+}$ energy transfer is found to be electric dipole–quadrupole interaction. The quantum efficiency of this transfer was estimated as being near to 100%, which makes these films interesting phosphors for the design of luminescent layers in flat-panel displays with two-colour emission.

1. Introduction

Aluminium oxide thin films have received considerable attention in recent years due to their possible applications as dielectric layers in various kinds of microelectronic devices [1, 2]. In particular, these films present high radiation resistance, high thermal conductivity, high chemical stability and low permeability to alkali impurities. These properties make them excellent candidates for applications as gate oxides in metal–oxide–semiconductor structures, e.g. as dielectric films in chemical sensors, passivation layers and hard coatings on several substrates [3, 4]. Moreover, Al_2O_3 can be an important component in thin film electroluminescent devices because of its wide energy band gap, and as an optical active layer in flat-panel displays [5], which require thin films with good luminescent properties and chemical stability. Wide band gap materials incorporating rare earth (RE) ions, such as Eu^{3+} [6], Tb^{3+} [7, 8] and Ce^{3+} [9], which emit through excitation–relaxation processes within their own energy levels, have turned out to be of great interest for these applications [10].

Flat-panel display applications require good quality materials emitting the three basic colours (blue, green and red). Efficient blue emitting material has been difficult to obtain, so at the present there continues an intensive research drive to resolve this problem [11]. Recently, efficient blue emission was achieved in $CeCl_3$ doped aluminium oxide films deposited by spray pyrolysis under specific deposition conditions (substrate temperature during deposition, amount of cerium mixed in the spraying solution and film stoichiometry) [9]. Spray pyrolysis is a low cost deposition technique suitable for large area deposition of thin films [12, 13]. On the other hand, red emission can be achieved by co-doping the film with ions emitting in this range of wavelengths, such as Mn^{2+}. In fact, although the Mn^{2+} d $\rightarrow$ d absorption transitions are forbidden by spin and parity for electric dipole radiation absorption, such ions can be efficiently sensitized by RE ions such as Ce^{3+} [14, 15]. Because it is important to find efficient blue and red emitting materials for the design of luminescent layers in flat-panel displays, in the present work the Ce^{3+}-sensitized Mn^{2+} luminescence in Al_2O_3:Ce^{3+}:Mn^{2+} films prepared by the spray pyrolysis technique is analysed. To our knowledge, this is the first work on Mn^{2+} luminescence sensitized by Ce^{3+} ions in Al_2O_3 films.

2. Experimental procedure

Al_2O_3 films doped with Ce^{3+} and/or Mn^{2+} ions were prepared using the spray pyrolysis technique [16]. In this technique a solution with appropriate reactive materials is sprayed through a spraying nozzle over a hot substrate at atmospheric pressure. The spraying solution was a 0.07 M solution of $Al_2Cl_3{\cdot}6H_2O$ dissolved in de-ionized water (18 MΩ cm^{-1}), and $CeCl_3$ and $MnCl_2$ (Aldrich Chemical Co.) were added as doping materials. The spray was produced by means of an ultrasonic generator at a frequency of 0.8 MHz. Filtered air was used as the transport gas, at a flow rate of 10 l min^{-1}. The solution was sprayed at a rate of 1 ml min^{-1}. Corning 7059 glass slides were used as substrates. The substrate temperature during the film deposition was 300 °C. The time of synthesis was 6 min for a film thickness of about 5 μm, as measured with a profilometer, Sloan Dektak IIA. The surface roughness of the films, as measured by the profilometer, turned out to be 0.66 ± 0.03 μm. The crystalline structure of the sample was analysed by x-ray diffractometry (XRD) using a 1.540 Å (Cu Kα) Siemens D5000 diffractometer, which was operated at 30 keV.

The chemical composition of the films was measured using energy dispersive spectroscopy (EDS) with a Leica Cambridge Electron Microscope model Stereoscan 440 equipped with a beryllium window x-ray detector.

Luminescence spectra were obtained with a Perkin-Elmer LS-50B spectrometer. Emission spectra after 254 nm excitation were recorded using an UV mercury lamp, 8 W model UVGL-25, so that the sample luminescence could be detected by means of an optical fibre coupled to the spectrometer operated in the bioluminescence mode. Lifetime data of the Mn^{2+} emission and time resolved spectra were obtained with this spectrometer operated in the phosphorescence mode. Lifetime measurements of the Ce^{3+} emission were carried out by exciting the sample at 355 nm with 10 ns pulses of a Lumonics HY-1200 third-harmonic Nd:YAG laser. The sample fluorescence was monitored by a 0.5 M Spex monochromator and a Hamamatsu R636 photomultiplier tube, and then processed by a Hewlett-Packard model 54201A digitizing oscilloscope.

All measurements were carried out at room temperature.

3. Results

3.1. EDS measurements

The chemical composition values measured from EDS spectra for the films deposited with solution concentrations of 5 and 10 at.% of $CeCl_3$ and 1, 3 and 5 at.% of $MnCl_2$ (with respect

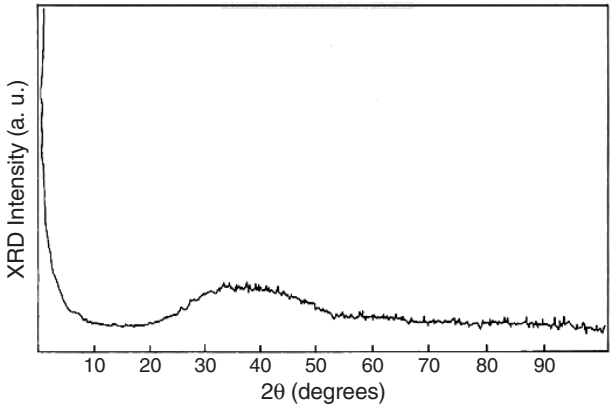

Figure 1. X-ray diffraction pattern of the AOC5M1 doubly doped film.

Table 1. Chemical composition of the films as measured by EDS.

	Solution concentration (at.%)		Chemical composition (at.%)				
Sample	$CeCl_3$	$MnCl_2$	O	Al	Cl	Ce	Mn
AOC5	5	0	55.49	34.48	6.65	3.38	0
AOC10	10	0	47.88	38.27	9.04	4.81	0
AOC5M1	5	1	57.72	33.27	6.11	2.72	0.18
AOC10M1	10	1	57.90	31.36	7.55	3.06	0.21
AOC10M3	10	3	50.50	37.10	7.54	4.01	0.85
AOM5	0	5	62.74	32.54	4.42	0	0.30

to the Al content) are listed in table 1. The films will be referred to hereafter in terms of their solution concentration as AOC5, AOC10, AOC5M1, AOC10M1, AOC10M3 and AOM5. It was found that the relative amount of chlorine in the films increases as the amount of $CeCl_3$ and $MnCl_2$ in the starting solution increases. This can be attributed to the production of residual chlorines during the solvent evaporation process, since the chemical reaction on the substrate surface on adding, for example, $CeCl_3$ and $MnCl_2$ might be [6]

$$2AlCl_3 + CeCl_3 + MnCl_2 + 3H_2O \rightarrow Al_2O_3:Ce^{3+}:Mn^{2+} + 6HCl \uparrow + nCl_2 \uparrow .$$

3.2. XRD measurements

The crystalline structure of the samples was monitored by XRD. All samples studied exhibited a very broad band without any indication of crystallinity, typical for amorphous materials. Figure 1 displays the diffraction pattern of the AOC5M1 doubly doped film, from which such a very broad band associated with a non-crystalline state can be observed.

The $Ce^{3+}(Al^{3+})$ and $Mn^{2+}(Al^{3+})$ substitution can, in principle, induce a substantial rearrangement of the nearest environment, which adjusts the space necessary to incorporate the Ce^{3+} (1.03 Å) and Mn^{2+} (0.80 Å) ions larger than the Al^{3+} ion (0.51 Å) [17, 18], and the divalent manganese charge compensation might be attained by residual chlorines.

3.3. Luminescence

The emission spectrum displayed by cerium singly doped films excited with ultraviolet light at 320 nm consists of a blue broad band, which is associated with strong inhomogeneous

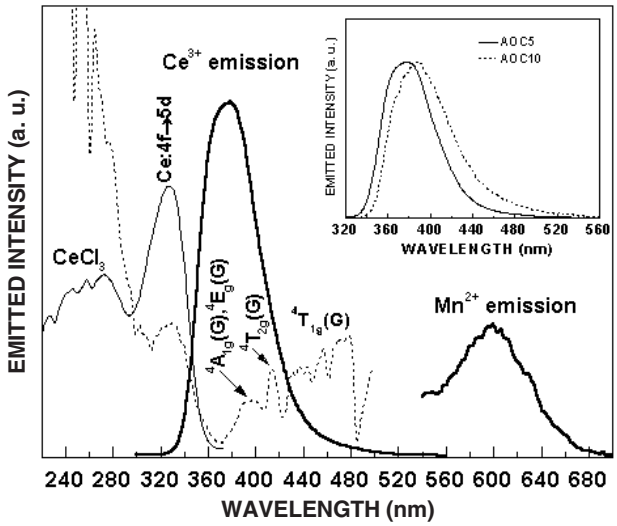

Figure 2. Excitation and emission spectra of the AOC5M1 doubly doped film. The excitation spectra were taken at $\lambda_{em} = 400$ nm (solid thin curve) and 600 nm (dashed curve). The emission spectra (solid thick curves) were obtained under excitation at 320 nm. The excitation spectrum taken at 600 nm and the Mn^{2+} emission spectrum were recorded with a delay time of 0.1 ms. The inset shows the normalized Ce^{3+} emission spectra for the AOC5 and AOC10 films.

broadening due to the amorphous structure of the films. The peak of this emission appears at 380 nm in AOC5 and it shifts toward larger wavelengths (390 nm) in AOC10 as can be appreciated from the AOC5 and AOC10 normalized emission spectra portrayed in the inset of figure 2. This behaviour of the blue emission is similar to the previously reported emission in aluminium oxide films doped with similar cerium concentrations [9] in the sense that it seems to be composed of two overlapping peaks. The relative intensity of these peaks depends on the amount of cerium in the film, so the lower energy peak becomes dominant as the cerium concentration is increased [9]. Thus, the blue emission can be attributed to the de-excitation of Ce^{3+} ions from the $^2D_{3/2}$ excited state to the split ground state, into their $^2F_{5/2}$ and $^2F_{7/2}$ components.

In addition to the blue emission of Ce^{3+} ions, a red emission could be obtained by co-doping the film with Mn^{2+} ions. Figure 2 shows excitation and emission spectra of the AOC5M1 doubly doped film. The emission spectrum, obtained under excitation at 320 nm, consists of the blue broad band characteristic of Ce^{3+} ions, peaking at ∼380 nm, and a red broad band peaking at ∼600 nm. The shape of the blue band is very similar to that observed in the AOC5 singly doped film excited with the same wavelength. The red emission was observed by recording the spectrum 0.1 ms after the excitation pulse, so that it becomes quite resolved from the Ce^{3+} blue emission. This red emission was observed only after the film was simultaneously doped with $MnCl_2$ and, therefore, it can be attributed to the Mn^{2+} $^4T_{1g}(G) \rightarrow {}^6A_{1g}(S)$ transition. On the other hand, the excitation spectra were taken at 400 nm (cerium emission) and 600 nm (manganese emission). The excitation spectrum corresponding to the Ce^{3+} emission consists of two broad bands centred at ∼257 and 320 nm (solid thin curve in figure 2). This spectrum is analogous as the one monitored at the same wavelength ($\lambda_{em} = 400$ nm) for the AOC5 singly doped film. The higher energy band (257 nm) is similar to that observed in cerium chloride powder [9] and, therefore, it can be attributed to $CeCl_3$ aggregates formed in the film. The 320 nm excitation band is similar to that previously observed for cerium doped aluminium

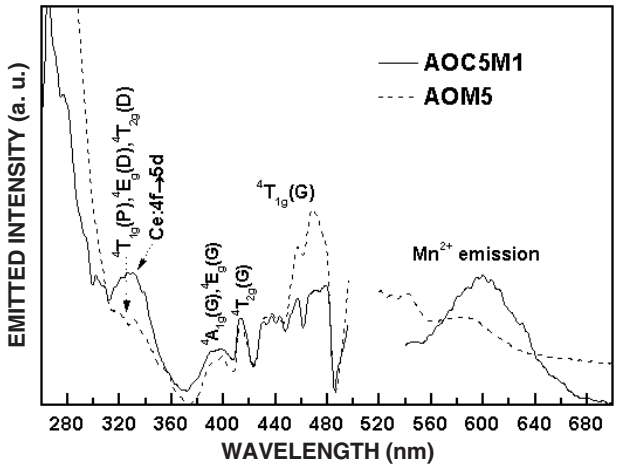

Figure 3. Excitation and Mn^{2+} emission spectra of the AOC5M1 and AOM5 films recorded with a delay time of 0.1 ms. The excitation spectra were taken at $\lambda_{em} = 600$ nm and the emission spectra were obtained under excitation at 320 nm.

oxide films [9] and, hence, it can be associated with transitions from the 4f to the 5d electronic energy levels of Ce^{3+} ions. The excitation spectrum of the red emission, recorded with a delay time of 0.1 ms, not only contains the $^6A_{1g}(S) \rightarrow {}^4T_{1g}(G)$, $^6A_{1g}(S) \rightarrow {}^4T_{2g}(G)$ and $^6A_{1g}(S) \rightarrow {}^4A_{1g}$, $^4E_g(G)$ Mn^{2+} absorption transitions, but also the 320 nm Ce^{3+} absorption band.

For comparison, figure 3 shows the excitation spectra of the red emission taken at 600 nm, as well as the Mn^{2+} emission spectra after excitation at 320 nm, displayed by the AOC5M1 and AOM5 films. In the doubly doped film the Ce^{3+} 4f $\rightarrow$ 5d excitation band stands out from the $^6A_{1g}(S) \rightarrow {}^4T_{1g}(P)$, $^4E_g(D)$ and $^4T_{2g}(D)$ Mn^{2+} transitions and a notable enhancement of the Mn^{2+} emission is observed, in spite of its quite low manganese concentration (0.18 at.%). On the other hand, in the AOM5 singly doped film the quite weak manganese emission becomes partially overlapped by the high background under the Mn^{2+} spectrum.

3.4. Lifetime measurements

Lifetime measurements performed on the Ce^{3+} emission observed in the films containing cerium were carried out monitoring the emission at 400 nm after 355 nm laser pulsed excitation. In the absence of Mn^{2+} ions the Ce^{3+} emission decay is exactly simple exponential, whereas in the presence of Mn^{2+} ions the decay is non-exponential, so it could be fitted to a double-exponential decay, with a time constant at long times close to the value obtained without transfer. The results obtained are listed in table 2. As an example, the Ce^{3+} emission decay curves and their fitting through exponential functions for the AOC10 and AOC10M3 films excited at 355 nm are portrayed in figure 4.

On the other hand, from lifetime measurements carried out on the Mn^{2+} emission at 600 nm under 320 nm excitation an exponential emission decay with a lifetime value of 1.7 ± 0.3 and 1.3 ± 0.2 ms in the AOC5M1 and AOC10M3 films, respectively, could be corroborated. This great difference between the Ce^{3+} and Mn^{2+} emission decay times allowed us to resolve the Mn^{2+} emission from the Ce^{3+} emission after 320 nm excitation using time resolved spectroscopy.

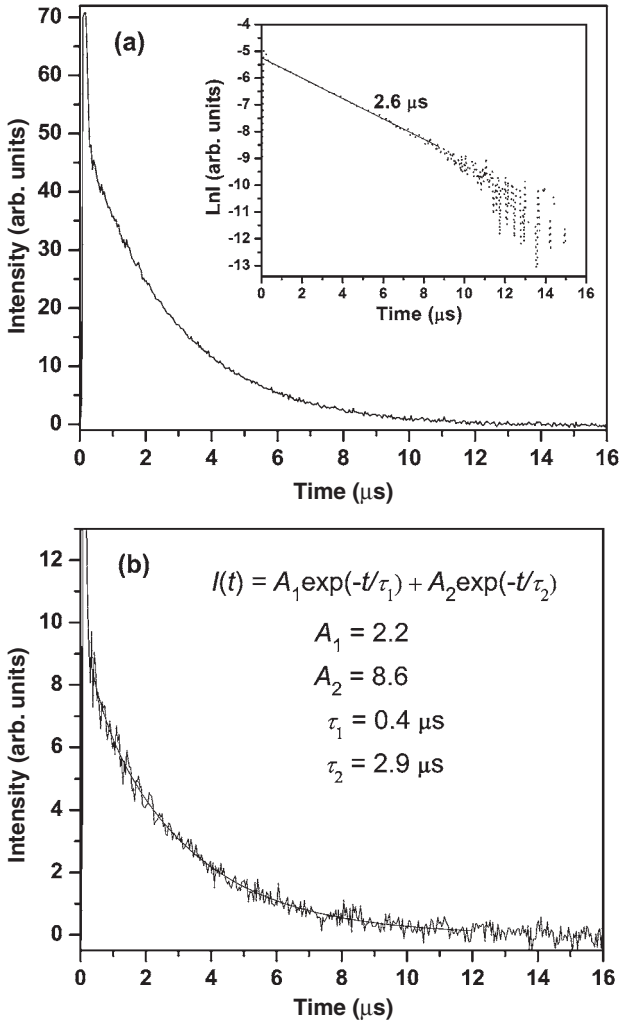

Figure 4. Ce^{3+} emission decay curves for the films (a) AOC10 and (b) AOC10M3 excited at 355 nm and λ_{em} = 400 nm. The linear fitting of the single-exponential decay in AOC10 and the double-exponential decay fitting in AOC10M3 are shown by the solid curves.

Table 2. Decay time constants of Ce^{3+} blue emission and Mn^{2+} red emission.

Film	λ_{exc} (nm)	λ_{em} (nm)	τ_{Ce} (μs)	τ_{Mn} (ms)
AOC5	355	400	2.4	
AOC10	355	400	2.6	
AOC5M1	320	600		1.7
	355	400	0.1[a]	
			2.6	
AOC10M3	320	600		1.3
	355	400	0.4[a]	
			2.9	

[a] Double-exponential decay.

4. Discussion

The presence of the 320 nm Ce^{3+} absorption band in the excitation spectrum of the Mn^{2+} emission, the enhancement of the Mn^{2+} emission after 320 nm excitation in AOC5M1 with

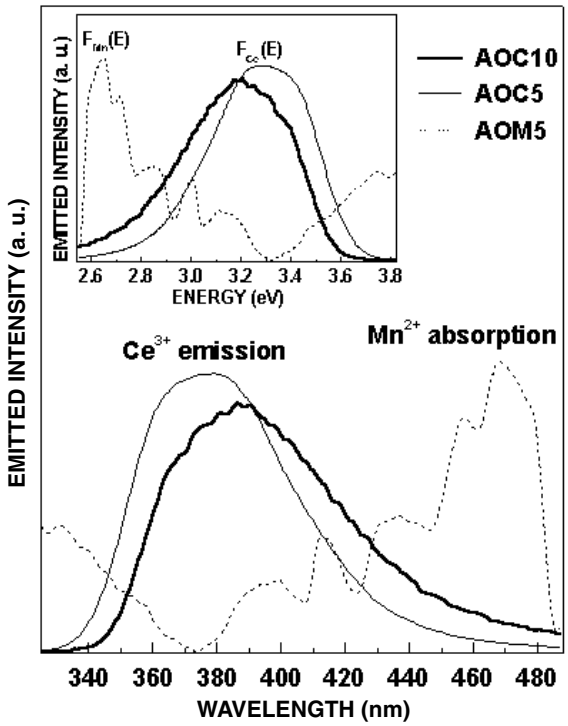

Figure 5. Overlap region of Mn^{2+} absorption (dashed curve) and Ce^{3+} emission (solid curves). The inset shows the normalized line-shape functions. The Mn^{2+} absorption spectrum was taken from the AOM5 excitation spectrum displayed in figure 3.

respect to that observed in AOM5 and the non-exponential nature of the Ce^{3+} emission decay in the presence of Mn^{2+} provide clear evidence that energy transfer from Ce^{3+} to Mn^{2+} ions occurs in the doubly doped film. This process is expected to occur taking into account that the cerium emission overlaps the Mn^{2+} $^6A_{1g}(S) \rightarrow {}^4T_{1g}(G)$, $^6A_{1g}(S) \rightarrow {}^4T_{2g}(G)$, $^6A_{1g}(S) \rightarrow {}^4A_{1g}$, $^4E_g(G)$, $^6A_{1g}(S) \rightarrow {}^4T_{2g}(D)$, $^6A_{1g}(S) \rightarrow {}^4E_g(D)$ and $^6A_{1g}(S) \rightarrow {}^4T_{1g}(P)$ absorption (excitation) transitions, as it can be appreciated from the normalized spectra portrayed in figure 5. The fact that the excitation spectrum of the Ce^{3+} emission in AOC5M1 is the same as that obtained in AOC5 indicates the absence of back energy transfer.

Although it is not possible to know the actual nature of the Ce^{3+}–Mn^{2+} interaction producing the energy transfer from Ce^{3+} to Mn^{2+} ions, it is expected that a short range interaction mechanism might be taking place for such ions. The short lifetime measured for the Ce^{3+} emission proves that the 4f $\rightarrow$ 5d absorption transition of the Ce^{3+} ions is electric dipole allowed. On the other hand, the long lifetime measured for the Mn^{2+} emission reveals the forbidden nature of the 3d $\rightarrow$ 3d transitions. Therefore, it is expected that the $Ce^{3+} \rightarrow Mn^{2+}$ energy transfer could occur via an electric dipole–quadrupole interaction mechanism.

The transfer rate W_{sa}^{DQ} for the electric dipole–quadrupole interaction between sensitizer (Ce^{3+}) and activator (Mn^{2+}) ions is related to the electric dipole–dipole transfer probability W_{sa}^{DD} through the following relationship [19]:

$$W_{sa}^{DQ} = \frac{f_q}{f_d}\left(\frac{\lambda_{Ce}}{R_{sa}}\right)^2 W_{sa}^{DD}, \tag{1}$$

Table 3. Calculated rates and quantum efficiencies of $Ce^{3+} \rightarrow Mn^{2+}$ energy transfer using electric multipolar interaction mechanisms (dipole–dipole and dipole–quadrupole) and Ce^{3+} intrinsic radiative decay rates ($1/\tau_{Ce}^{o}$) in the AOC5M1 and AOC10M3 films.

Film	$1/\tau_{Ce}^{o}$ (s^{-1})	W_{sa}^{DD} (s^{-1})	W_{sa}^{DQ} (s^{-1})	η^{DD} (%)	η^{DQ} (%)
AOC5M1	4.2×10^5	1.0×10^5	8.6×10^7	19.4	99.5
AOC10M3	3.8×10^5	1.6×10^5	1.5×10^8	29.4	99.7

where λ_{Ce} is the wavelength position of the cerium emission, R_{sa} is the interaction distance between the Ce^{3+} and Mn^{2+} ions involved in the energy transfer, f_q ($\sim 10^{-10}$) and f_d ($\sim 10^{-7}$) are the oscillator strengths of the Mn^{2+} ion electric quadrupole and dipole transitions, respectively. The expression for W_{sa}^{DD} is [19]

$$W_{sa}^{DD} = \frac{3\hbar^4 c^4}{4\pi n^4 \tau_{Ce}^{o}} \left(\frac{1}{R_{sa}}\right)^6 Q_{Mn}\Omega, \tag{2}$$

where n is the refractive index of the host medium, τ_{Ce}^{o} is the Ce^{3+} ion intrinsic lifetime in the absence of Mn^{2+} ions, Q_{Mn} is the oscillator strength of the Mn^{2+} absorption transitions, which are in resonance with the Ce^{3+} emission transition, and $\Omega = \int [F_{Ce}(E) F_{Mn}(E)/E^4]\,dE$ is the spectral overlap integral of the normalized line-shape functions of the Ce^{3+} emission $F_{Ce}(E)$ and Mn^{2+} absorption $F_{Mn}(E)$, E being the transfer energy. The remaining symbols in equation (2) have their usual meaning. Because the optical absorption spectrum of Mn^{2+} ions was hardly detectable, due to the forbidden nature of their transitions, even at very high resolution conditions of the optical spectrophotometer, the manganese integrated absorption coefficient was estimated using the relationship $Q_{Mn} = 4.8 \times 10^{-20}$ eV $m^2 \cdot f_d$, derived by Blasse [20]. The overlap integral was calculated using the functions $F_{Ce}(E)$ and $F_{Mn}(E)$ in the overlap region, which are shown in the inset of figure 5. The function $F_{Mn}(E)$ was obtained from the excitation spectrum of the 600 nm Mn^{2+} emission displayed by the AOM5 film (figure 3). Thus, Ω was found to be 4.3×10^{-3} and 6.4×10^{-3} eV^{-5} for AOC5M1 and AOC10M3, respectively. Therefore, in AOC10M3 the overlap between the Ce^{3+} emission and Mn^{2+} excitation line functions is greatly improved because the Ce^{3+} emission moves further to the lower energy side.

The energy transfer rates W_{sa}^{DQ} and W_{sa}^{DD} found from equations (1) and (2) for the AOC5M1 and AOC10M3 films, in which the Ce^{3+}–Mn^{2+} spacing can be taken as $R_{sa} \approx 4.1$ and 4.0 Å, respectively, are given in table 3. The Ce^{3+} intrinsic radiative decay rates ($1/\tau_{Ce}^{o}$) for both films are also included in the table for comparison. The R_{sa} interaction distances were roughly estimated from the Ce^{3+} and Mn^{2+} amounts determined by EDS for each film assuming a uniform ion distribution. As expected, an electric dipole–quadrupole interaction mechanism is quite a lot more probable than the electric dipole–dipole one. In fact, the W_{sa}^{DD} transfer rate is lower than the Ce^{3+} intrinsic radiative decay rate. It can also be noted that for AOC10M3 the transfer rates are higher than for AOC5M1 as a consequence of the better overlap between the Ce^{3+} emission and Mn^{2+} absorption (excitation).

The R_{sa}^{o} critical interaction distance between Ce^{3+} and Mn^{2+} ions for energy transfer, that is, the distance at which the energy transfer rate is equal to the Ce^{3+} ion intrinsic decay rate ($W_{sa}^{DQ}\tau_{Ce}^{o} = 1$), was estimated from equations (1) and (2), using the values found for Ω and that estimated for Q_{Mn}. These distances turned out to be ~8 Å (8.0 Å in AOC5M1 and 8.4 Å in AOC10M3). Therefore, the R_{sa} distance (~4 Å) is smaller than the R_{sa}^{o} distance. From this finding along with the fact that the overlap of the normalized Ce^{3+} emission and Mn^{2+} absorption (excitation) is quite good and similar to those found in other systems [14, 15], an efficient $Ce^{3+} \rightarrow Mn^{2+}$ energy transfer can be expected.

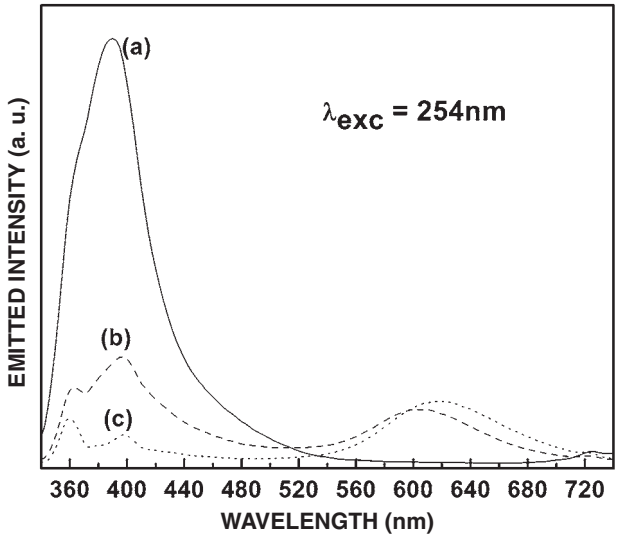

Figure 6. Emission spectra of the (a) AOC10, (b) AOC10M1 and (c) AOC10M3 films excited with an UV mercury lamp at 254 nm.

The quantum yield of energy transfer η from Ce^{3+} to Mn^{2+} ions can provide information on whether the Ce^{3+} ion acts as a good sensitizer to Mn^{2+} ions. Taking into account that

$$\eta = \frac{W_{sa}}{1/\tau_{Ce}} \tag{3}$$

and

$$W_{sa} = 1/\tau_{Ce} - 1/\tau_{Ce}^{o}, \tag{4}$$

we have [21, 22]

$$\eta = \frac{W_{sa}\tau_{Ce}^{o}}{1 + W_{sa}\tau_{Ce}^{o}}. \tag{5}$$

So the quantum efficiency of energy transfer for an electric dipole–dipole or dipole–quadrupole interaction mechanism can be evaluated from equation (5). The values of η obtained for the AOC5M1 and AOC10M3 films are listed in table 3. A quantum yield near to 1 is obtained for an electric dipole–quadrupole interaction, which indicates that the Mn^{2+} red emission can be sensitized by Ce^{3+} ions with efficiency near to 100%. This quite high efficiency is evidenced by the strong reduction of the Ce^{3+} emission intensity in the presence of manganese (figure 4). In fact, such an intensity reduction is even more evident for doubly doped films excited at 254 nm with an UV mercury lamp. Figure 6 portrays emission spectra recorded for the AOC10, AOC10M1 and AOC10M3 films excited at 254 nm. In addition to the red emission being observed on co-doping the film with manganese, the Ce^{3+} emission in the AOC10M1 and AOC10M3 films becomes partially and completely quenched, respectively. Thus, the emissions observed from the AOC10M1 and AOC10M3 films excited with the short wavelength line (254 nm) of an UV mercury lamp appear eye red–blue and eye red only, respectively.

5. Summary and conclusions

A blue–red emission phosphor under ultraviolet light excitation can be manufactured with Al_2O_3:Ce^{3+}:Mn^{2+} films deposited by the spray pyrolysis technique. These emissions have been attributed to the 5d → 4f de-excitation of Ce^{3+} ions (blue emission) and 3d → 3d de-excitation of Mn^{2+} ions (red emission). The intense blue emission is a broad band including the two transitions from the 5d-excited state to the $^2F_{5/2}$ and $^2F_{7/2}$ components of the ground state. This luminescence feature has an advantage for display techniques, which require a purer blue emission. The weak red emission observed in the AOM5 manganese singly doped film is found to be quite enhanced through an efficient energy transfer from Ce^{3+} to Mn^{2+} ions in the AOC5M1 doubly doped film. The spectroscopic data obtained suggest that the energy transfer occurs through a short range interaction mechanism. An electric dipole–quadrupole interaction seems to be the most probable mechanism occurring in the Ce^{3+}–Mn^{2+} complexes. The quantum yield of energy transfer was estimated as being near to 100%, which makes these Al_2O_3:Ce^{3+}:Mn^{2+} films interesting phosphors for the design of luminescent layers in flat-panel displays emitting simultaneously in two of the three basic colours (blue and red).

Acknowledgments

The work was supported by CONACyT under projects No 43016-F and No G37858-E. The authors thank J Guzmán and L Baños for technical support in EDS and XRD measurements. Also, the technical assistance of J García-Coronel, M Guerrero, A Soto, M Flores and A Lira is acknowledged. R Martínez gratefully acknowledges the CONACyT grant No 163802. The authors are grateful to the referees for the critical reading of the manuscript and for their useful suggestions.

References

[1] Aguilar-Frutis M, García M and Falcony C 1998 *Appl. Phys. Lett.* **72** 1700
[2] Kolodzey J, Chowdhury E, Adam T, Qui G, Rau I, Olowolafe J, Suehle J and Chen Y 2000 *IEEE Trans. Electron. Devices* **47** 121
[3] Gustin K M and Gordon R G 1988 *J. Electron. Mater.* **17** 509
[4] Saraie J and Ngan S 1990 *Japan. J. Appl. Phys.* 1 **29** 1877
[5] Tannas E L 1985 *Flat Panel Displays and CRT* (New York: Van Nostrand-Reinhold)
[6] Martínez E, García M, Ramos-Brito F, Álvarez-Fregoso O, López S, Granados S, Chávez-Ramírez J, Martínez R M and Falcony C 2000 *Phys. Status Solidi* b **220** 677
[7] Falcony C, Ortíz A, Domínguez J M, Farías M H, Cota-Araiza L and Soto G 1992 *J. Electrochem. Soc.* **139** 267
[8] Esparza-García A E, García-Hipólito M, Aguilar-Frutis M A and Falcony C 2003 *J. Electrochem. Soc.* **150** H53
[9] Falcony C, García M, Ortiz A, Miranda O, Gradilla I, Soto G, Costa-Araiza L, Farias M H and Alonso J C 1994 *J. Electrochem. Soc.* **141** 2860
[10] Benalloul P and Benoit J 1991 *Luminescence—Phenomena, Materials and Devices* ed R P Rao (Commack, NY: Nova Science)
[11] Depp S W and Howard W E 1993 *Sci. Am.* **266** 40
[12] Jergel M, Conde-Gallardo A, García M and Falcony C 1998 *Appl. Phys. Lett.* **72** 1700
[13] Ortiz A, García M, Sánchez A and Falcony C 1989 *J. Electrochem. Soc.* **136** 1232
[14] Caldiño U G 2003 *J. Phys.: Condens. Matter* **15** 3821
[15] Caldiño U G 2003 *J. Phys.: Condens. Matter* **15** 7127
[16] Langlet M and Joubert J C 1992 *Chemistry of Advanced Materials* ed C N R Rao (Oxford: IV-PAC-Blackwell) pp 55–79
[17] Low W and Suss J T 1960 *Phys. Rev.* **119** 132
[18] Kaplyanskii A A, Kulinkin A B, Kutsenko A B, Feofilov S P, Zakharchenya R I and Vasilevskaya T N 1998 *Phys. Solid State* **40** 1310
[19] Dexter D L 1953 *J. Chem. Phys.* **21** 836
[20] Blasse G 1969 *Philips Res. Rep.* **24** 131
[21] Kumar G A, Biju P R, Jose G and Unnikrishnan N V 1999 *Mater. Chem. Phys.* **60** 247
[22] Paulose P I, Jose G, Thomas V, Unnikrishnan N V and Warrier M K R 2003 *J. Phys. Chem. Solids* **64** 841